An Investigation of the Unusual ^{57}Fe Mössbauer Quadrupole Splittings and Isomer Shifts in 2 and 3-Coordinate Fe(II) Complexes

Yong Zhang and Eric Oldfield*

Departments of Chemistry and Biophysics, University of Illinois at Urbana-Champaign, 600 South Mathews Avenue, Urbana, Illinois 61801

Received: February 10, 2003; In Final Form: April 26, 2003

The ^{57}Fe Mössbauer quadrupole splittings (ΔE_Q) and isomer shifts (δ_{Fe}) in 3-coordinate high-spin Fe(II) complexes are unusually small, and previous attempts to reproduce their ΔE_Q values have been unsuccessful. We show here that, by using large structural models and basis sets, both ΔE_Q and δ_{Fe} values can be quite accurately predicted by using density functional theory. Four systems were investigated: the three 3-coordinate species $[LFeX]^0$ (L = β-diketiminate; X = Cl^-, CH_3^-) and $[Fe(SC_6H_2\text{-}2,4,6\text{-}t\text{Bu}_3)_3]^-$, in addition to an uncommon 2-coordinate high-spin ferrous thiolate, $[Fe(SC_6H_3\text{-}2,6\text{-mes}_2)_2]$ (mes = mesityl = 2,4,6-$Me_3C_6H_2$). Both Gaussian-type-orbital and Slater-type-orbital basis sets were investigated, and both yielded ΔE_Q and δ_{Fe} values in good accord with experiment. There were no improvements in these property predictions when (approximate) relativistic effects were included in the calculations. An MO analysis provided a detailed picture of the origin of the small ΔE_Q values seen in the 3-coordinate complexes. These results extend the scope of DFT/Mössbauer investigations beyond the 4−6-coordinate systems described previously to 2- and 3-coordinate systems, which should open the way to using these parameters in structure refinement, especially in large systems, such as proteins.

Introduction

Iron−sulfur proteins are common to all life forms and have many diverse functions, for example, in electron transfer, in catalysis, and in iron and oxygen sensing.[1−3] Among these multiple functions, the role of Fe−S proteins in biological N_2 reduction by nitrogenase has generated considerable interest, leading to numerous chemical, biochemical, spectroscopic, and theoretical investigations.[4−12] The active site of nitrogenase contains an iron−molybdenum cofactor in which the seven iron atoms have been thought, at least until recently,[12] to be 3-coordinate. Since 3-coordinate iron is rather uncommon, there have been considerable synthetic efforts expended on the synthesis of 3-coordinate iron complexes, together with many spectroscopic studies aimed at elucidating their electronic structures.[13−15] Mössbauer spectroscopy is potentially a particularly powerful technique in this respect, since the Mössbauer transition of the ^{57}Fe isotope[16] is readily observed and can yield useful information on the charge density and the electric field gradient (EFG) at the iron nucleus. The main ^{57}Fe Mössbauer spectroscopic observables are the isomer shift (δ_{Fe}) and the quadrupole splitting (ΔE_Q). In many high-spin ferrous complexes, ΔE_Q values are ∼3 mm s^{-1}, while δ_{Fe} values are ∼1 mm s^{-1}.[16,17] However, these values are much smaller ($\Delta E_Q \approx$ 0.7 mm s^{-1} and δ_{Fe} = 0.41 mm s^{-1}, at 100 K)[18] in the $MoFe_7S_9$ cofactor cluster of nitrogenase, which contains four to six ferrous sites.[19,20] Early crystallographic studies of nitrogenase revealed a close to planar 3-coordinate $[FeS_3]$ structure for Fe in the FeMo cofactor, and this stimulated the synthesis of a series of 3-coordinate Fe(II) complexes, including one which had unusually small ΔE_Q ((−)0.81 mm s^{-1}) and δ_{Fe} (0.57 mm s^{-1}) values.[15] However, attempts at reproducing the Mössbauer ΔE_Q values in these model systems were not successful, and it has been proposed that making accurate ab initio predictions of ΔE_Q in these systems is virtually impossible.[13] Here, we reinvestigate the calculation of the ^{57}Fe Mössbauer ΔE_Q and δ_{Fe} values in three 3-coordinate Fe(II) complexes and one 2-coordinate Fe(II) complex and demonstrate that these properties can in fact be successfully predicted using DFT methods when using large basis sets and structural models. We also probe the orbital interactions which lead to these unusual Mössbauer properties, some of which can be expected to contribute to the unusual Mössbauer observables seen in the FeMo cofactor of nitrogenase in which planar FeS_3 subunits now appear to be slightly distorted due to interaction with a fourth ligand, most likely N (resulting in N−Fe−S bond angles of ∼102°).[12]

Computational Aspects

The Mössbauer quadrupole splitting is related to the components of the electric field gradient tensor at the nucleus as follows:[16]

$$\Delta E_Q = \frac{1}{2} e Q V_{zz} \left(1 + \frac{\eta^2}{3}\right)^{1/2} \tag{1}$$

where e is the electron charge, Q is the quadrupole moment of the $E^* = 14.4$ keV excited state, and the principal components of the EFG tensor are labeled according to the convention

$$|V_{zz}| > |V_{yy}| > |V_{xx}| \tag{2}$$

with the asymmetry parameter being given by

$$\eta = \frac{V_{xx} - V_{yy}}{V_{zz}} \tag{3}$$

The Mössbauer isomer shift is given by[16]

10.1021/jp030177q CCC: $25.00
Published on Web 06/26/2003

$$\delta_{Fe} = E_a - E_{Fe} = \frac{2\pi}{3} Ze^2(\langle R^2\rangle^* - \langle R^2\rangle)(|\psi(0)|_A{}^2 - |\psi(0)|_{Fe}{}^2) \quad (4)$$

where Z represents the atomic number of the nucleus of interest (iron) and R and R^* are average nuclear radii of the ground and excited states of ^{57}Fe. Since $|\psi(0)|_{Fe}{}^2$ is a constant, the isomer shift (from Fe) can be written as

$$\delta_{Fe} = \alpha[\rho(0) - c] \quad (5)$$

where α is the so-called calibration constant and $\rho(0)$ is the computed charge density at the iron nucleus. Both α and c can be obtained from the correlation between experimental δ_{Fe} values and the corresponding computed $\rho(0)$ data in a training set, and are dependent on the quantum chemical method used and the choice of basis set.[21] Then, one can use eq 5 to predict δ_{Fe} for a new molecule from its computed $\rho(0)$, basically as described in detail elsewhere for a wide variety of heme and other model systems.[21]

To calculate ΔE_Q, we first used the Gaussian 98 program[22] and Gaussian-type-orbital (GTO) basis sets to evaluate the principal components of the electric field gradient tensor at the ^{57}Fe nucleus (V_{ii}), as described previously.[23−25] We then used the Amsterdam density functional (ADF) 2002 program[26] and Slater-type-orbital (STO) basis sets to again evaluate the iron EFG, to make a comparison between the two different basis set treatments. This comparison was made since STO-based basis sets have a better cusp behavior than do GTO-based basis sets. We used eq 1 to deduce ΔE_Q using a precise recent determination[27] of $Q = 0.16$ ($\pm$5%) $\times 10^{-28}$, a value previously found to permit excellent accord between theory and experiment in a broad range of both diamagnetic[24,25] and paramagnetic[23] systems.

We also used the output data from both the Gaussian 98 program[22] and the ADF 2002 program[26] to evaluate the charge density at the iron nucleus, $\rho(0)$, which determines the ^{57}Fe Mössbauer isomer shift. In the former case, we read the wave functions from the Gaussian 98 calculations into the AIM 2000 program[28] to obtain $\rho(0)$, while we used the "densf" utility in the ADF program[26] to get $\rho(0)$ in the latter case.

In the Gaussian 98 calculations, we used the same computational approach as used in our previous Mössbauer and NMR hyperfine shift studies.[21,23,29] A Wachter's basis (62111111/3311111/3111)[30] was used for Fe, 6-311G* for all the other heavy atoms, and 6-31G* for hydrogens. We also investigated use of both the pure density functional BPW91 (Becke 88 exchange[31] and PW91[32] correlation functionals) as well as the hybrid functional B3LYP (Becke's three-parameter functional[33] with the LYP[34] correlation functional). The α and c values were those deduced previously, and are shown below for each functional:[21]

$$\delta_{Fe} = -0.471[\rho(0) - 11617.30] \quad \text{(BPW91)} \quad (6)$$

$$\delta_{Fe} = -0.404[\rho(0) - 11614.16] \quad \text{(B3LYP)} \quad (7)$$

Additional calculations were also carried out to study the effects of basis set size, counterion charge, and cluster size/truncation.

In the ADF calculations, the pure DFT functional BPW91 and the largest basis set available (TZ2P, triple ζ with two polarization functions) were used. There is no hybrid DFT method available in the ADF 2002 program.[26] However, the ADF program does have the capability of treating relativistic effects using two different approximations: Pauli and ZORA (zero-order regular approximation).[35] Comparing the Gaussian 98 and ADF calculations thus enables one to probe the effects of functional type and basis set type and, in addition, relativistic effects on the computed properties.

We computed ΔE_Q and δ_{Fe} values for three 3-coordinate complexes, $[LFeX]^0$ (L = β-diketiminate; X = Cl^- (**1**), CH_3^- (**2**)) and $[Fe(SC_6H_2\text{-}2,4,6\text{-}t\text{Bu}_3)_3]^-$ (**3**), Figure 1, in addition to an uncommon 2-coordinate high-spin ferrous thiolate, $[Fe(SC_6H_3\text{-}2,6\text{-mes}_2)_2]$ (mes = mesityl = 2,4,6-$Me_3C_6H_2$) (**4**; Figure 1), which has an unexpectedly small isomer shift but a normal quadrupole splitting.[15] This species is thought to be a possible model for a 2-coordinate FeMo cofactor intermediate. To minimize the influence of any structure truncations on the theoretical results, we only replaced the R = CH_3 groups in Figure 1 with hydrogens. This resulted in much larger structural models than those used in other DFT studies.[13] In particular, the 3-coordinate systems **1**, **2**, and **3** have 539, 537, and 679 basis functions, respectively, while the 2-coordinate complex **4** has 801 basis functions, in the Gaussian 98 calculations. The spin-unrestricted method was used for each system. Calculations were performed by using Silicon Graphics (Mountain View, CA) O-300 and O-2000 computers, using eight or sixteen processors, respectively. The tight convergence (10^{-8} au) criterion of the SCF calculations was selected in Gaussian 98,[22] while default settings (10^{-6} au) were used in the ADF program.[26] MO visualizations were made by using the Cerius[2] program.[37]

Results and Discussion

The computational results from the Gaussian 98 calculations (using GTO basis functions and no relativistic effects) are given in Table 1. The Mulliken spin densities on the iron atoms in all four complexes are consistent with their high-spin ($S = 2$) nature, although they are somewhat smaller than those found previously in the $S = 2$ iron hemes:[23] 3.48 vs 3.79 using the BPW91 functional and 3.62 vs 3.80 using the B3LYP functional, on average. There is, therefore, a larger ligand contribution to the MOs containing the unpaired electrons in these four complexes, in accord with conclusions drawn from a previous study.[13]

To assess the performance of these computational methods on the low-coordinate iron complexes **1**−**4**, and to compare these results with those obtained previously for 4−6-coordinate iron complexes,[21,23] we show in Figures 2 and 3 a comparison between experimental and computed ΔE_Q and δ_{Fe} results for **1**−**4** with those found for the higher coordinate complexes. The BPW91 results shown in Figure 2A are for the title compounds **1**−**4** only (●), while in Figure 2B these points are shown superimposed on BPW91 results for the 23 species computed previously (○). There is clearly an excellent correlation between theory and experiment for **1**−**4** ($R^2 = 0.982$, root-mean-square error (rmse) 0.37 mm s^{-1}, slope 1.14, and intercept −0.07 mm s^{-1}). When all data points ($N = 27$) are considered together, the correlation (solid line in Figure 2B) is again excellent ($R^2 = 0.975$, rmse = 0.31 mm s^{-1}, slope 1.02, and intercept −0.10 mm s^{-1}). For the B3LYP calculations, there is also very good agreement with experiment for **1**−**4**, Figure 2C, and the computed ΔE_Q values fall close to the correlation line (shown solid, Figure 2D) which can be drawn through all the data points ($R^2 = 0.978$, $N = 27$, rmse = 0.29 mm s^{-1}, slope = 1.12, and intercept = −0.25 mm s^{-1}). In contrast to these results, we show in Figure 2C,D the results of DFT ΔE_Q calculations using the B3LYP functional, but on a smaller structural model (structure 2 in ref 13) and with a smaller (6-311G) basis set. These computed results for **1** and **2** (square symbols in Figure 2C,D)

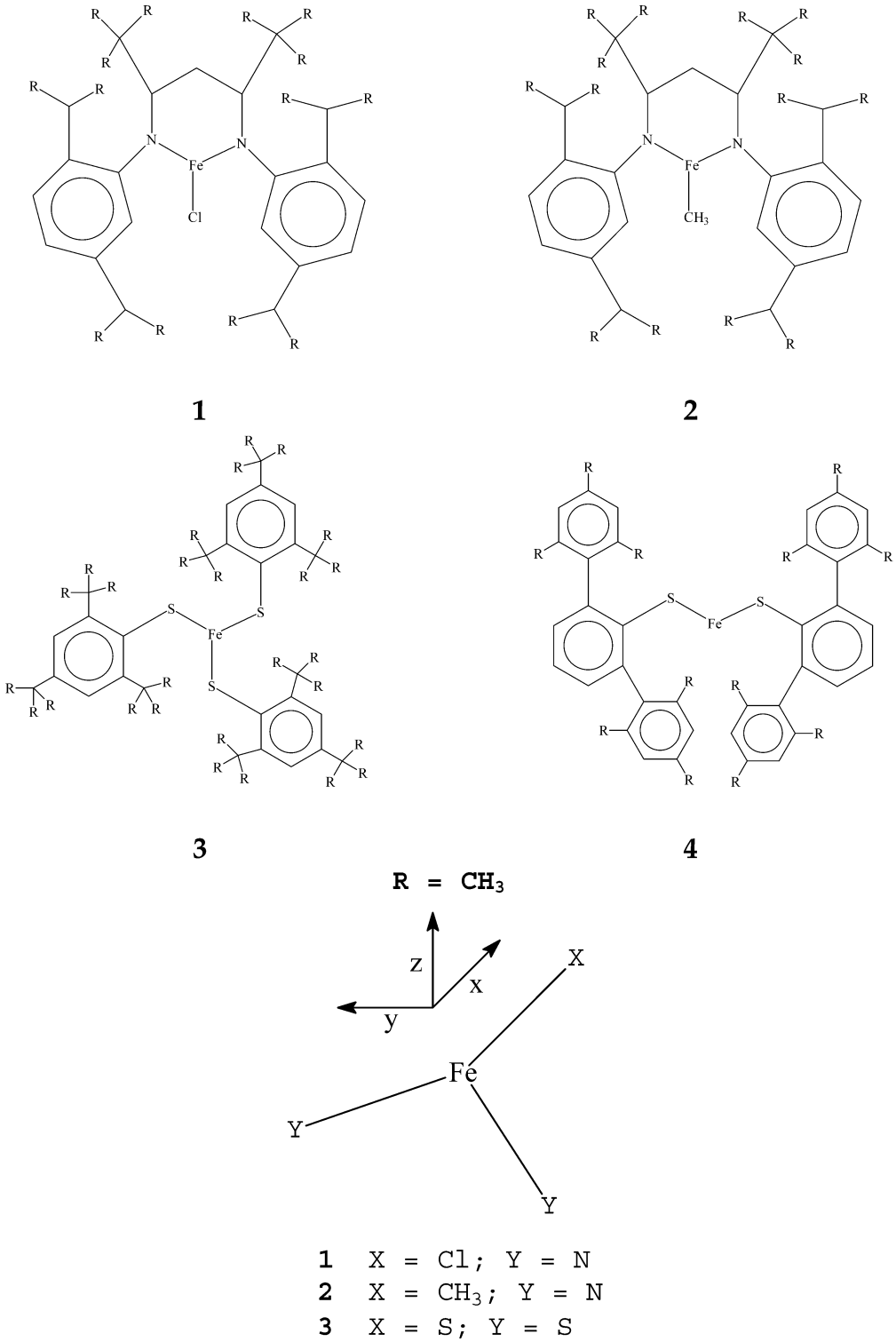

Figure 1. Structures of the complexes studied in this work and the Cartesian coordinate systems for the 3-coordinate compounds (**1**−**3**).

have the wrong ΔE_Q sign and are considerably off the correlation line we find for both **1**−**4** and all the heme and other model compounds. Thus, large basis set schemes and a large structural model appear to be necessary for evaluating ΔE_Q values in such Fe(II) complexes, and indeed, side chain orbital contributions are found to be present in some frontier MOs in these complexes (vide infra). When all data points for the 2- and 3-coordinate species **1**−**4** plus the 4−6-coordinate hemes investigated previously are considered, the entire range of experimental ΔE_Q values increases to 6.87 mm s^{-1}, and the overall rms error in prediction is 0.31 (0.29) mm s^{-1} with R^2 values of 0.975 (0.978) for the BPW91 (B3LYP) functional. There is thus only a ∼4% rms error over the whole ΔE_Q range using the methods we have described above.

The relatively small δ_{Fe} values of all four high-spin ferrous complexes[13,15] are also satisfactorily reproduced in the calculations, as shown in Table 1 and Figure 3, using either functional. When solely **1**−**4** are considered, the R^2 value for the experiment-versus-theory correlation is 0.960 with an rmse = 0.033 mm s^{-1} for the BPW91 calculations (Figure 3A). These results are compared with the results of previous calculations on the Mössbauer isomer shifts in a variety of iron complexes,

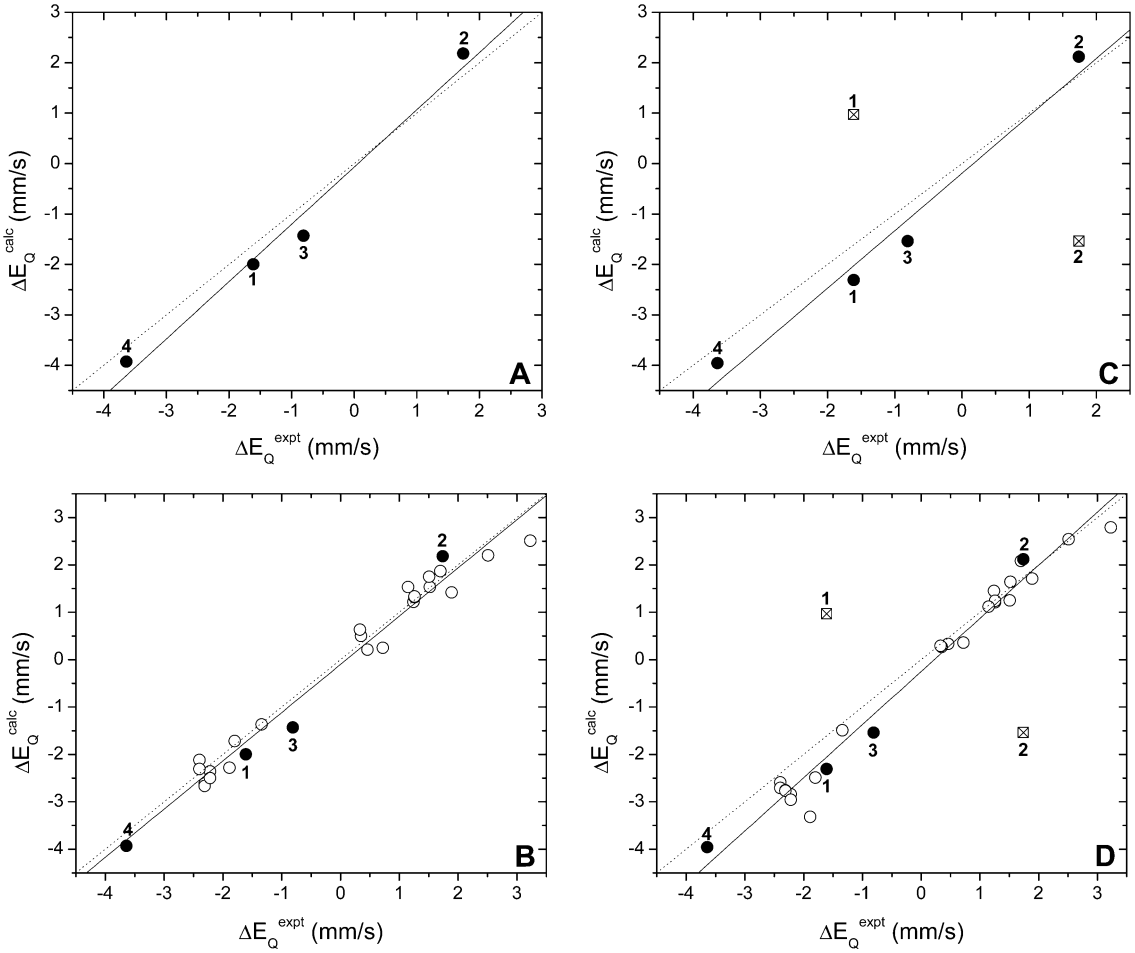

Figure 2. Nonrelativistic DFT/GTO ΔE_Q computational results plotted versus the experimental ΔE_Q results: (A) BPW91 (**1**−**4** only); (B) BPW91 (**1**−**4** (●) plus 23 other models (from ref 23) (○)); (C) B3LYP (**1**−**4** only); (D) B3LYP (**1**−**4** (●) plus 23 other models (from ref 23) (○)). The solid lines are the best-fit lines through either the **1**−**4** results (●) (A and C) or all data points (● and ○) (C and D). The dotted line is the ideal 45° line with a slope of 1.00 and an intercept of 0.00 mm s^{-1}. The results of B3LYP/6-311G calculations for **1** and **2** based on structure 2 in ref 13 are shown by square symbols.

TABLE 1: Nonrelativistic DFT/GTO Calculations in Some High-Spin Ferrous Complexes

complex	method	ΔE_Q (mm s^{-1})	δ_{Fe} **(mm s^{-1})**	$\rho(0)$ (au)	$\rho_{\alpha\beta}$(Fe)[a] (e)
1	expt[b]	−1.61	0.74		
	BPW91	−2.00	0.75	11615.71	3.54
	B3LYP	−2.31	0.72	11612.39	3.65
	B3LYP[c]	−0.97		11615.90	3.63
2	expt[b]	+1.74	0.48		
	BPW91	+2.18	0.43	11616.39	3.67
	B3LYP	+2.12	0.40	11613.17	3.77
	B3LYP[c]	−1.54		11616.64	3.67
3	expt[d]	(−)0.81	0.57		
	BPW91	−1.43	0.61	11616.01	3.33
	B3LYP	−1.54	0.55	11612.80	3.53
4	expt[d]	(−)3.64	0.75		
	BPW91	−3.93	0.79	11615.63	3.36
	B3LYP	−3.96	0.73	11612.35	3.53

[a] Mulliken spin density on iron. [b] Both the experimental values and the signs of the Mössbauer observables are from ref 13. [c] Result calculated by using B3LYP and a 6-311G basis on structure 2 reported in ref 13. [d] The values of the Mössbauer observables are from ref 15. The ΔE_Q signs were not determined in the experiments and are thus shown here in parentheses, based on the theoretical results, since these methods have successfully reproduced the ΔE_Q signs in a wide range of other diamagnetic and paramagnetic iron complexes (see refs 23−25).

including inorganic, organometallic, and metalloprotein/metalloporphyrin model systems, in Figure 3B. When all 2−6-coordinate species are considered, we find an $R^2 = 0.973$ and an rmse = 0.075 mm s^{-1} for all 28 structures investigated, covering a range in δ_{Fe} of 2.34 mm s^{-1}. This represents only a ∼3% rms error over the entire range. Moreover, when the B3LYP functional is used, there is a further improvement: $R^2 = 0.986$ and rmse = 0.019 mm s^{-1} for **1**−**4** (Figure 3C) and $R^2 = 0.981$ and rmse = 0.064 mm s^{-1} for all 28 structures considered (Figure 3D).

These results clearly demonstrate that it is now possible to quite accurately predict both ^{57}Fe Mössbauer ΔE_Q and δ_{Fe} values by using high-quality large-scale spin-unrestricted DFT techniques. The EFG property in general appears to be somewhat more difficult to predict and is more basis set dependent. For example, using the same large structural models as shown in Figure 1, a smaller basis (6-311G) calculation on **4** produced an incorrect sign (data not shown) and a much worse slope, although this basis does appear to produce good correlations ($R^2 = 0.945$ and 0.984 for BPW91 and B3LYP, respectively) between computed $\rho(0)$ and experimental δ_{Fe} values for these four complexes (data not shown). This is consistent with our previous systematic δ_{Fe} studies[21] and the results of δ_{Fe} calculations on iron−sulfur proteins,[11] in which a triple-ζ STO basis set was used.

To further investigate whether the proposed computational models (especially the basis set scheme) we refined previously for reproducing Mössbauer isomer shifts, quadrupole splittings,

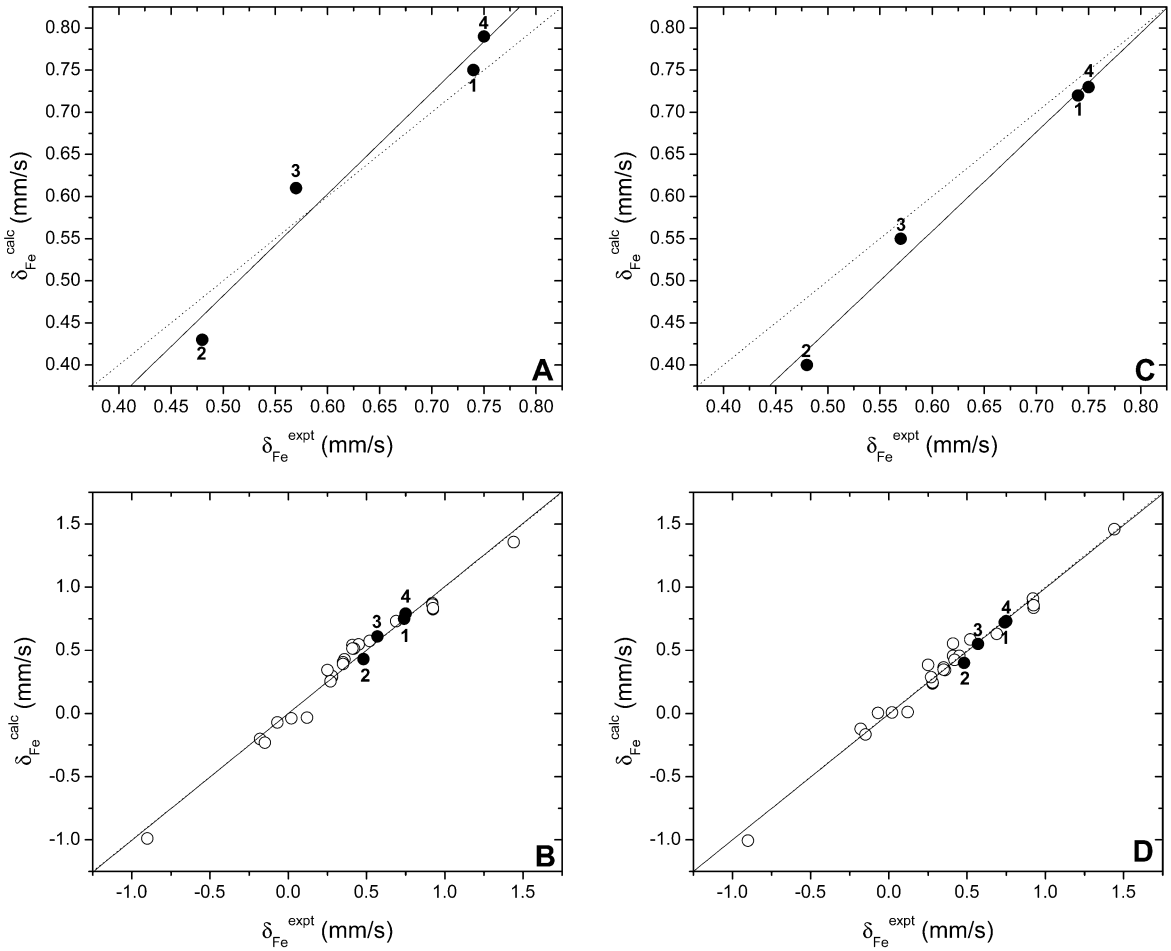

Figure 3. Nonrelativistic DFT/GTO computational results plotted versus the experimental data for δ_{Fe}: (A) BPW91 (**1**−**4** only); (B) BPW91 (**1**−**4** (●) plus 24 other model compounds (ref 21) (○)); (C) B3LYP (**1**−**4** only); (D) B3LYP (**1**−**4** (●) plus 24 other model compounds (ref 21) (○)). The solid lines are the best-fit lines through either the **1**−**4** results (●) (A and C) or all of the data points on the graph (C and D). The dotted line is the ideal 45° line with a slope of 1.00 and an intercept of 0.00 mm s^{-1}.

and NMR hyperfine shifts in a wide range of paramagnetic 4−6-coordinate hemes and model systems[21,23,29] are also optimized for these 2−3-coordinate nitrogenase model systems, we carried out a series of calculations on the planar, high-spin, 3-coordinate iron thiolate complex **3**, $[Fe(SC_6H_2\text{-}2,4,6\text{-}t\text{Bu}_3)_3]^-$. This has a very small experimental ΔE_Q value, and its computed ΔE_Q has the largest absolute deviation from experiment, Table 1. We considered three effects: basis set size, counterion charge, and cluster size/truncation effects. We first added one diffuse function and one additional polarization function to the original basis for the sulfur atoms, which are directly bonded to the iron center. As shown in Table 2, this 6-311+G(2d) basis had essentially no effects on ΔE_Q or δ_{Fe} predictions using either functional; neither did using the largest Pople-type basis set for sulfur in Gaussian 98[22] (6-311+G(3df)), although use of 6-311+G(3df) put slightly more spin density on the iron. These results strongly suggest that our basis set for predicting Mössbauer observables is well optimized. However, considering that structural model **3** has a negative charge, while the other complexes studied in this work are neutral, it appeared that it might be desirable to incorporate a counterion in the calculation. However, incorporating a $[PMe_4]^+$ ion (at the P lattice position of $[PPh_4]^+$ in the crystal structure) had no effect, as shown in Table 2, which in retrospect seems reasonable since the charge centers are well separated.[15] Next, we evaluated the effect of the size of the structural model used in the calculations. To see whether the structure for complex **3** (see Figure 1), in which R (=Me) groups were replaced by hydrogens, is sufficient or not, we performed additional calculations using both functionals on a much larger cluster. Specifically, instead of having *o*-methyl substituents, we utilized *o*-isopropyl groups, incorporating those methyl groups which were closest to the iron. This model has 943 basis functions, to be compared with the 679 basis functions used in the original model, but again this had essentially no

TABLE 2: Effect of Additional Theoretical Treatments on the Prediction of the Mössbauer Observables of High-Spin 3-Coordinate Iron−Thiolate Complex 3

method	additional treatment	ΔE_Q (mm s^{-1})	δ_{Fe} (mm s^{-1})	$\rho_{\alpha\beta}$(Fe)[a] (e)
BPW91	none[b]	−1.43	0.61	3.33
	1[c]	−1.44	0.61	3.33
	2[d]	−1.42	0.60	3.39
	3[e]	−1.43	0.62	3.33
	4[f]	−1.42	0.57	3.32
B3LYP	none[b]	−1.54	0.55	3.53
	1[c]	−1.55	0.55	3.55
	2[d]	−1.53	0.54	3.59
	3[e]	−1.55	0.55	3.53
	4[f]	−1.48	0.51	3.52

[a] Mulliken spin density on iron. [b] No additional treatment: results from Table 1. [c] As footnote *b* but 6-311+G(2d) for S atoms. [d] As footnote *b* but 6-311+G(3df) for S atoms. [e] As footnote *b* but the counterion (PPh_4^+) in the crystal was considered and modeled as PMe_4^+. [f] *o*-Isopropyl groups used on the phenyl rings with methyl groups chosen to be those which were closest to the iron.

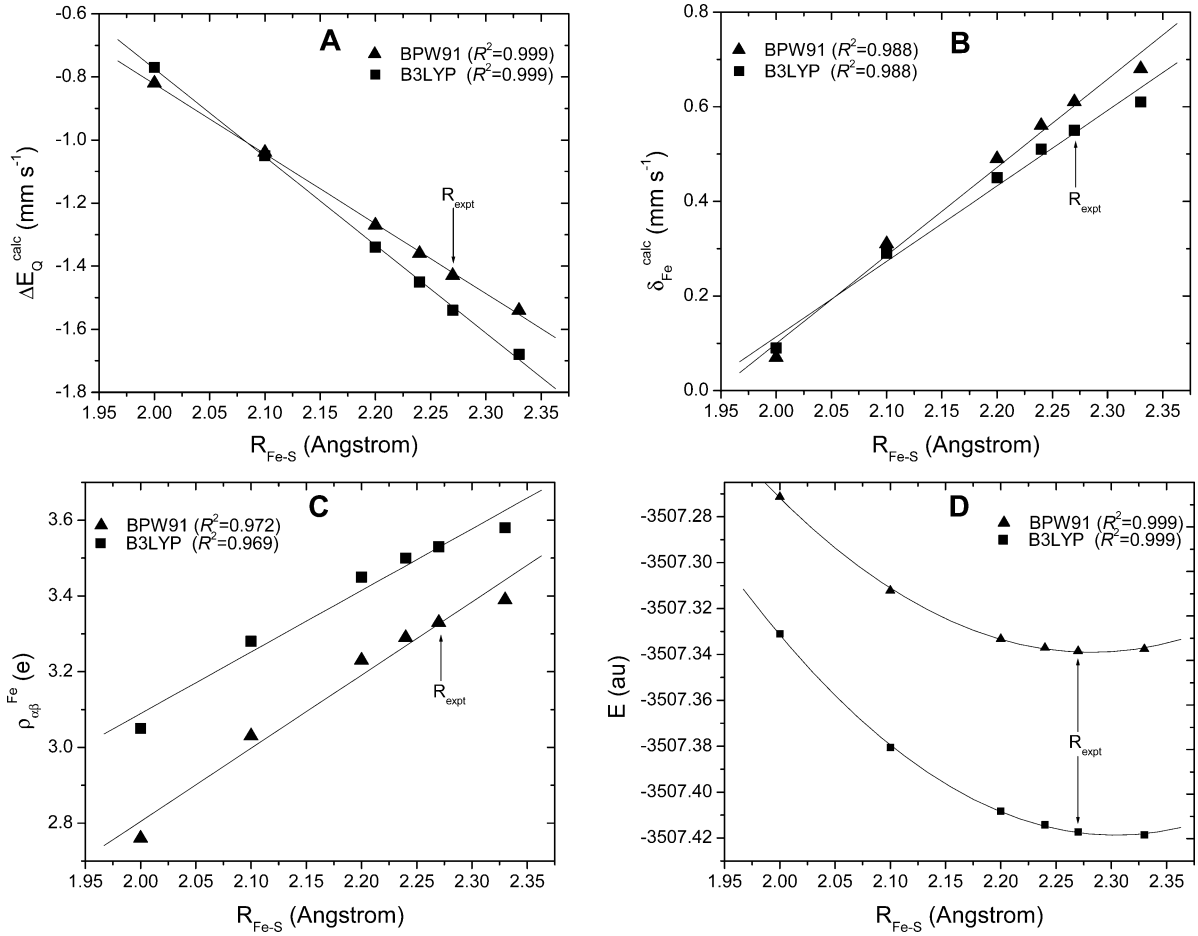

Figure 4. Distance effects on DFT-computed electronic properties for complex **3**: (A) ΔE_Q; (B) δ_{Fe}; (C) $\rho_{\alpha\beta}^{Fe}$; (D) E. For the first three properties, the data points were fitted to straight lines using linear regression: the correlation coefficients (R^2) are indicated on the graphs. In (D), a parabolic curve was drawn through the data: the correlation coefficients are again shown on the graph. The experimental R_{Fe-S} is indicated as R_{expt} on the graphs.

effect on the ΔE_Q results (see Table 2). The residual errors might come from neglect of second-order Doppler effects, as well as from uncertainties in the quality of the crystallographic structures, as discussed previously.[23] In addition, it might also be that neglect of relativistic effects would be important, as discussed below.

To assess the sensitivity of ΔE_Q and δ_{Fe} (and $\rho_{\alpha\beta}^{Fe}$) to Fe−S bond length variations (or uncertainties), we evaluated each of these properties at five additional R_{Fe-S} distances. The results are shown in Figure 4, together with computed values for the total energy. The experimental R_{Fe-S} is indicated in Figure 4 as R_{expt}. There is a linear relationship between both the Mössbauer quadrupole splitting (Figure 4A) and isomer shift (Figure 4B) with Fe−S distance. Upon decreasing the Fe−S bond length, the iron−ligand interaction increases the ligand contributions to the final wave function. The calculated absolute ΔE_Q values become smaller (more positive), as shown in Figure 4A, with slopes of −2.22 and −2.80 (mm s^{-1})/Å for BPW91 and B3LYP functional calculations, respectively. This is again in good accord with the idea of large ligand contributions to the EFG in these systems.[13] The enhanced ligand contribution also increases the charge density at the iron nucleus, thereby reducing δ_{Fe}, as may be seen in Figure 4B, where the slopes are 1.86 and 1.60 (mm s^{-1})/Å for BPW91 and B3LYP functionals, respectively. The iron spin densities decrease with decreasing Fe−S distance, as shown in Figure 4C, again consistent with an increasing ligand contribution at short Fe−S bond lengths. The electronic energies have, as expected, a parabolic dependence on the Fe−S distance, as shown in Figure 4D. The experimental geometry (R_{Fe-S} = 2.27 Å)[15] is seen to have the lowest energy (within an uncertainty of ∼1 kcal/mol) using either functional, and the δ_{Fe} values at this geometry are almost exactly those found experimentally. However, ΔE_Q is still ∼0.6 mm s^{-1}, at variance with the experimental result.

TABLE 3: BPW91/STO Calculations of Mössbauer Observables with and without Relativistic Treatment

complex	relativistic treatment	ΔE_Q (mm s^{-1})	δ_{Fe} (mm s^{-1})	$\rho_{\alpha\beta}$(Fe)[a] (e)
1	none	−2.06	11820.99	3.61
	Pauli	−2.07	13887.98	3.64
	ZORA	−2.04	12850.30	3.63
2	none	+2.22	11821.62	3.77
	Pauli	+2.26	13889.59	3.80
	ZORA	+2.19	12851.28	3.81
3	none	−1.35	11821.36	3.36
	Pauli	−1.33	13931.62	3.38
	ZORA	−1.47	12850.84	3.39

[a] Mulliken spin density on iron.

We therefore next investigated the incorporation of relativistic effects (Pauli and ZORA formalisms[35]) on ΔE_Q and δ_{Fe} predictions for **1**−**3**, since these compounds have unusually small ΔE_Q values. The results are shown in Table 3. In addition, use of the ADF program also allowed us to compare the effects of using STOs versus GTOs, since ADF calculations utilize STO basis functions, which have better cusp behavior. Only the BPW91 functional was considered, since the hybrid functional is not available in the ADF program.

Without relativistic corrections, the Mulliken spin densities on the iron atoms in these 3-coordinate complexes from the BPW91/STO calculations indicate their high-spin ($S = 2$) nature, as also found in the BPW91/GTO calculations. In fact, the BPW91/STO-derived $\rho_{\alpha\beta}^{Fe}$ values parallel the BPW91/GTO results ($R^2 = 1.000$), although they are slightly larger. The Mössbauer quadrupole splittings predicted by using the ADF DFT/STO approach shown in Table 3 are very close ($R^2 = 0.999$) to those obtained by using the DFT/GTO approach, shown in Table 1. It should be noted that the largest basis set (TZ2P) was used throughout the ADF calculations, but there is no improvement over use of GTO functions. In addition, the charge densities at the iron nucleus in compounds **1**−**3**, computed by using the BPW91/STO ADF approach, also exhibit a very good correlation with the GTO (Gaussian 98) results, when the same functional is used: $R^2 = 0.972$.

The ΔE_Q results using both types of relativistic correction shown in Table 3 are very similar to those found in the nonrelativistic calculations. This could suggest only a small relativistic effect on the EFG, and indeed, even fully relativistic Dirac−Hartree−Fock calculations show only a small effect on iron EFG predictions in organometallic complexes.[39] For **1**−**3**, the recommended ZORA method in ADF[26,35] shows slightly better agreement with the Gaussian 98 calculations ($R^2 = 1.000$, rms deviation 0.005 mm s^{-1}) than do the results of the Pauli treatment ($R^2 = 0.999$, rms deviation 0.113 mm s^{-1}), but clearly there are no major differences from the nonrelativistic calculations.

On the other hand, the relativistic effects on the charge density at the iron nucleus in these systems (see Table 3) are noticeable. Compared to $\rho(0)$ data without any relativistic treatment ($\sim 1.2 \times 10^4$ au), the ZORA treatment enhances $\rho(0)$ to $\sim 1.3 \times 10^4$ au, which further increases to $\sim 1.4 \times 10^4$ au using the Pauli treatment. For comparison, fully relativistic Dirac calculations[40] yield $\sim 1.5 \times 10^4$ au for $\rho(0)$. So, relativistic effects are manifest in $\rho(0)$. However, as long as there is an excellent correlation between δ_{Fe} and $\rho(0)$ for a given theoretical method, the Mössbauer isomer shifts can be accurately predicted, even though the absolute $\rho(0)$ values may be 15−20% smaller. This important point has been discussed in detail by us before,[21] and has also been discussed by other groups.[11,41] By comparing the $\rho(0)$ results in Tables 1 and 3, it can also be seen that the $\rho(0)$ values in the ZORA calculations (BPW91/STO) have a good correlation with the results of the nonrelativistic BPW91/GTO calculations for **1**−**3** ($R^2 = 0.984$), suggesting that they might also be used to predict δ_{Fe}. However, the Pauli-type relativistic calculations in these high-spin, trigonal, ferrous complexes are poorly correlated with experiment.

We next investigate the role that the ligands play in contributing to the small δ_{Fe} and unusually small ΔE_Q values in the high-spin 3-coordinate Fe(II) complexes. We consider first the FeN_2X complexes (X = Cl, **1**; X = Me, **2**) and then the FeS_3 complex **3**. The computed spin densities of these nominally $S = 2$ systems (see Table 1) clearly show a smaller spin density on the iron center than is observed in other, more conventional high-spin ferrous systems.[23] This suggests a more significant ligand contribution. And, since these DFT calculations give a good account of the ΔE_Q and δ_{Fe} observables, it seems reasonable to believe that the wave functions are quite accurate, in which case it should be possible to use an MO analysis to probe these questions in more depth, basically as reported previously for a range of heme model systems.[23,29] In particular, we are interested in comparing the MO results from these DFT calculations with the results of a previous crystal field analysis[13] to try to determine, for example, the origins of the differences in ΔE_Q observed between complexes **1** and **2**, where the only structural differences are the presence of a Cl^- in **1** and a CH_3^- in **2**, which results, however, in $\Delta E_Q = -1.61$ (**1**) and $+1.74$ (**2**) mm s^{-1} values.

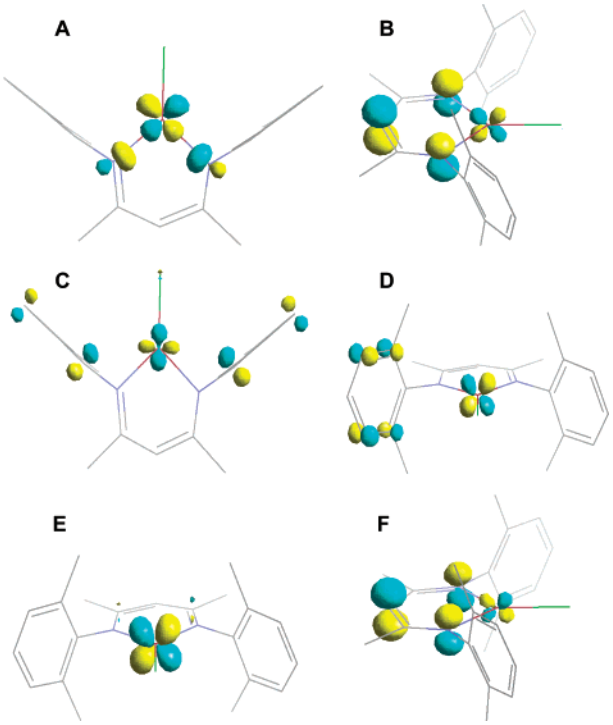

Figure 5. Isosurface representations of the frontier molecular orbitals for complex **1**: (A) α HOMO; (B) α HOMO − 1; (C) α HOMO − 2; (D) α HOMO − 3; (E) β HOMO; (F) β HOMO − 1 (contour values ±0.1 au).

The crystal field model produces the same picture as the frontier MO approach for **1** and **2**,[13] putting the four unpaired electrons in iron 3d orbitals with an energy order of $d_{xy} > d_{x^2-y^2} > d_{xz} > d_{yz}$. Our DFT calculations produce more detailed MO results, however, as shown, for example, in Figures 5 and 6. The four iron 3d orbitals are again found to be occupied by the four unpaired electrons ($S = 2$), and the α HOMOs of both **1** and **2** are the same, consisting of the iron d_{xy} orbital (Figures 5A and 6A), indicating that the crystal field and DFT analyses have the same general MO features. However, the current DFT results also show that there are extensive ligand contributions to these frontier molecular orbitals, in accord with the suggestion of a large ligand contribution made in the experimental investigation.[13] There are even side chain orbitals in some frontier MOs in these complexes (see Figure 5 in particular), indicating the complexity of the electronic properties in these systems and consequently the necessity of using large structural models. Since the third ligands (Cl^- in **1**, Me^- in **2**) are different in these two β-diketiminates, the DFT results show different MO features, which are likely to be responsible for the different EFG features seen in these two complexes, and which are not accounted for by a simple crystal field picture.[13] For example, despite the common characteristics of the α HOMOs, α MOs containing d_{xz} have a different ordering. Also, the other two MOs containing unpaired electrons exhibit different types of ligand interactions. In complex **2**, the third ligand (CH_3^-) makes an obvious contribution to its α HOMO − 1 (Figure 6B). On the other hand, no Cl^- orbital contribution is found in any of the four singly occupied 3d orbitals, Figure 5A−D. There is a large ligand contribution for sites directly bonded to iron, which

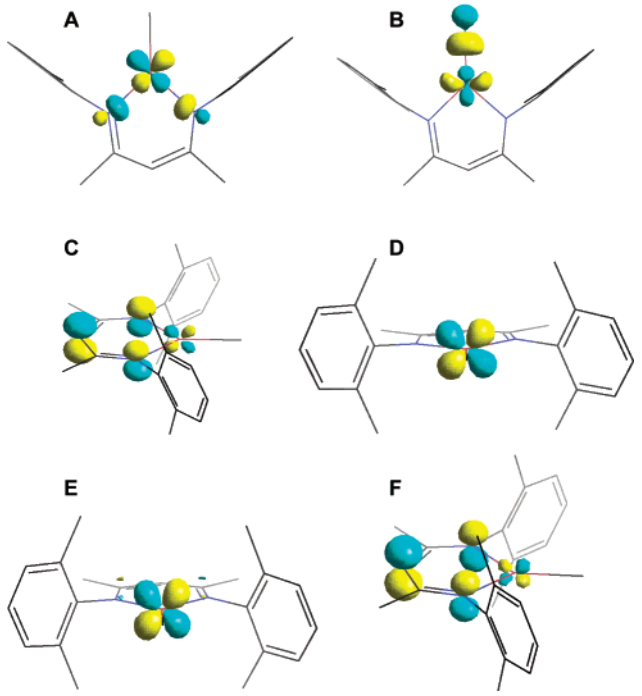

Figure 6. Isosurface representations of the frontier molecular orbitals for complex **2**: (A) α HOMO; (B) α HOMO − 1; (C) α HOMO − 2; (D) α HOMO − 3; (E) β HOMO; (F) β HOMO − 1 (contour values ±0.1 au).

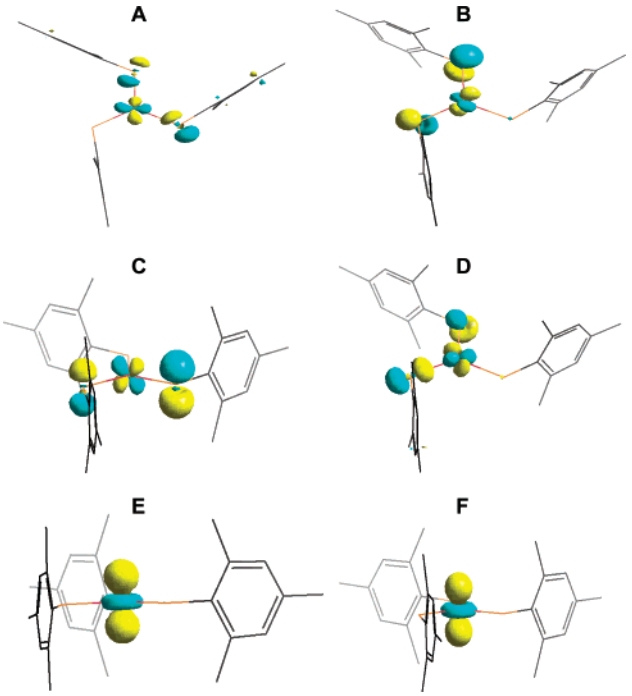

Figure 7. Isosurface representations of the frontier molecular orbitals for complex **3**: (A) α HOMO; (B) α HOMO − 1; (C) α HOMO − 2; (D) α HOMO − 3; (E) α HOMO − 4; (F) β HOMO (contour values ±0.08 au).

increases the charge density at iron and thereby reduces δ_{Fe} more in **2** (0.48 mm s^{-1}) than in **1** (0.74 mm s^{-1}).[13] The presence of a strong electron-donating ligand (CH_3^-) in the direct bonding sites in the *xy* plane and in the frontier MOs could also be a possible reason for the much more positive ΔE_Q observed for **2** (+1.74 mm s^{-1}) than for **1** (−1.61 mm s^{-1}),[13] since in general more electron density in the *xy* plane of the EFG principal axis system makes V_{zz} (ΔE_Q) more positive,[16] and in these complexes the EFG principal axis system obtained in the DFT calculations was found to basically coincide with the Cartesian coordinate system shown in Figure 1. The structural difference between these two high-spin iron β-diketiminates also results in a different energy level ordering among the d orbitals. In **2**, the ordering is $d_{xy} > d_{x^2-y^2} > d_{xz} > d_{yz}$, the same as predicted by the crystal field model.[13] But in **1**, $d_{x^2-y^2}$ is lower than d_{xz}, since $d_{x^2-y^2}$ in **1** (see Figure 5C) is almost nonbonding when compared to the stronger σ antibonding interaction of the CH_3^- orbitals with $d_{x^2-y^2}$ in **2** (see Figure 6B). The d_{xz} interactions in both complexes are about the same. The β frontier MOs are very similar in both molecules, as shown in Figures 5E,F and 6E,F. For these two complexes, although our calculations support the crystal field analysis in putting d_{xy}, $d_{x^2-y^2}$, d_{xz}, and d_{yz} in energetically higher states than d_{z^2},[13] our results do not put d_{z^2} immediately after these four α orbitals, or the β HOMO (Figures 5E and 6E).

The structural core of complex **3** has a symmetry (C_{3h}) different from those of **1** and **2**, and has the following frontier MO ordering, based on the crystal field analysis:[13] e′ (d_{xy}, $d_{x^2-y^2}$) > e″ (d_{xz}, d_{yz}) > a′ (d_{z^2}). This result is also basically reproduced in the DFT calculations, as shown in Figure 7. The four unpaired electrons in this high-spin ferrous system occupy two sets of degenerate MOs: α HOMO/α HOMO − 1 and α HOMO − 2/α HOMO − 3. d_{z^2} is found to immediately follow the other four iron 3d orbitals for both α- and β-type orbitals (Figure 7E,F). The $d_{x^2-y^2}$ (α HOMO) and d_{yz} (α HOMO − 2) orbitals can be clearly seen in Figure 7A,C, but the d_{xy} (α HOMO − 1) and d_{xz} (α HOMO − 3) orbitals are slightly canted (Figure 7B,D). It should also be noted that these DFT-derived MOs again show the importance of ligand contributions, as found for the 3-coordinate iron β-diketiminates. The difference now is that there is significant ligand character in the direct iron bonding sites in each of these four orbitals in complex **3**, while one or two of these orbitals in **1** and **2** do not contain any significant ligand character. As a result, the quadrupole splitting of **3** is the smallest of those observed.

Conclusions

The results we have described above are of interest for a number of reasons. First, we have found that the unusual ^{57}Fe Mössbauer quadrupole splittings and isomer shifts in 2- and 3-coordinate high-spin iron−thiolate complexes[15] and model systems[13] can be quite accurately calculated using spin-unrestricted DFT methods, as long as large-scale basis sets and structural models are used. For an overall data set containing 2−6-coordinates complexes we find $R^2 = 0.975$ (0.978) and a ∼4% rmse (BPW91, B3LYP) for ΔE_Q ($N = 27$) and $R^2 = 0.973$ (0.981) and a ∼3% rmse (BPW91, B3LYP) for δ_{Fe} ($N = 28$). Second, our results show that use of either GTO or STO basis sets can generate good predictions for both Mössbauer quadrupole splittings and isomer shifts, but there is no apparent advantage in using STO basis sets over GTO basis sets. Third, we investigated the utility of approximate treatments of relativistic effects using the Pauli and ZORA formalisms. Both produced similar ΔE_Q results but offered no advantage over nonrelativistic ΔE_Q predictions. However, the relativistic treatments did affect the absolute values of $\rho(0)$. Only the ZORA formalism was found to yield correctly ordered $\rho(0)$ values, and this approach may have potential in predicting δ_{Fe} values. Fourth, our MO investigations provide a firm theoretical basis for the experimental proposal of an important ligand contribution to the unusual EFGs[13] seen in planar, high-spin, 3-coordinate iron complexes.

When taken together, the results described above clearly indicate that large-scale spin-unrestricted nonrelativistic DFT methods can quite accurately predict the unusually small[13] Mössbauer quadrupole splittings in 3-coordinate Fe(II) systems, as well as provide accurate predictions of the small Mössbauer isomer shifts in both 2- and 3-coordinate complexes. This success can be expected to lead to more quantitative investigations of the geometric and electronic structures of paramagnetic metalloproteins and model systems.

Acknowledgment. This work was supported by the United States Public Health Service (NIH Grant EB 00271-24) and by the National Computational Science Alliance (Grant MCB-030008N).

References and Notes

(1) Beinert, H.; Holm, R. H.; Münck, E. *Science* **1997**, *277*, 653−659.

(2) Cowan, J. A. *Inorganic Biochemistry*; Wiley-VCH: New York, 1997.

(3) Holm, R. H.; Kennepohl, P.; Solomon, E. I. *Chem. Rev.* **1996**, *96*, 2239−2314.

(4) Kim, J.; Rees, D. C. *Nature* **1992**, *360*, 553−560.

(5) Kim, J.; Rees, D. C. *Science* **1992**, *257*, 1677−1682.

(6) Chan, M. K.; Kim, J.; Rees, D. C. *Science* **1993**, *260*, 792−794.

(7) Chen, J.; Christiansen, J.; Campobasso, N.; Bolin, J. T.; Titsworth, R. C.; Hales, B. J.; Rehr, J. J.; Cramer, S. P. *Angew. Chem., Int. Ed. Engl.* **1993**, *32*, 1592−1594.

(8) Kim, J.; Woo, D.; Rees, D. C. *Biochemistry* **1993**, *32*, 7104−7115.

(9) Peters, J. W.; Stowell, M. H. B.; Soltis, S. M.; Finnegan, M. G.; Johnson, M. K.; Rees, D. C. *Biochemistry* **1997**, *36*, 1181−1187.

(10) Mayer, S. M.; Lawson, D. M.; Gormal, C. A.; Roe, S. M.; Smith, B. E. *J. Mol. Biol.* **1999**, *292*, 871−891.

(11) Lovell, T.; Li, J.; Liu, T.; Case, D. A.; Noodleman, L. *J. Am. Chem. Soc.* **2001**, *123*, 12392−12410.

(12) Einsle, O.; Tezcan, F. A.; Andrade, S. L. A.; Schmid, B.; Yoshida, M.; Howard, J. B.; Rees, D. C. *Science* **2002**, *297*, 1696−1700.

(13) Andres, H.; Bominaar, E. L.; Smith, J. M.; Eckert, N. A.; Holland, P. L.; Münck, E. *J. Am. Chem. Soc.* **2002**, *124*, 3012−3025 and references therein.

(14) Smith, J. M.; Lachicotte, R. J.; Holland, P. L. *Chem. Commun.* **2001**, 1542−1543.

(15) MacDonnell, F. M.; Ruhlandt-Senge, K.; Ellison, J. J.; Holm, R. H.; Power, P. P. *Inorg. Chem.* **1995**, *34*, 1815−1822 and references therein.

(16) Debrunner, P. G. In *Iron Porphyrins*; Lever, A. B. P., Gray, H. B., Eds.; VCH Publishers: New York, 1989; Vol. 3, pp 139−234.

(17) Münck, E. *Methods Enzymol.* **1978**, *54*, 346−379. Münck, E. *Physical Methods in Inorganic and Bioinorganic Chemistry*; University Science Books: Sausolito, CA, 2000; Chapter 6, pp 287−319.

(18) Zimmermann, R.; Münck, E.; Brill, W. J.; Shah, V. K.; Henzl, M. T.; Rawling, J.; Orme-Johnson, W. H. *Biochim. Biophys. Acta* **1978**, *537*, 185−207. Huynh, B. H.; Münck, E.; Orme-Johnson, W. H. *Biochim. Biophys. Acta* **1979**, *576*, 192−203. Huynh, B. H.; Henzl, M. T.; Christner, J. A.; Zimmermann, R.; Orme-Johnson, W. H.; Münck, E. *Biochim. Biophys. Acta* **1980**, *623*, 124−138.

(19) Yoo, S. J.; Angove, H. C.; Papaefthymiou, V.; Burgess, B. K.; Münck, E. *J. Am. Chem. Soc.* **2000**, *122*, 4926−4936.

(20) True, A. E.; Nelson, M. J.; Venters, R. A.; Orme-Johnson, W. H.; Hoffman, B. M. *J. Am. Chem. Soc.* **1988**, *110*, 1935−1943.

(21) Zhang, Y.; Mao, J.; Oldfield, E. *J. Am. Chem. Soc.* **2002**, *124*, 7829−7839.

(22) Frisch, M. J.; Trucks, G. W.; Schlegel, H. B.; Scuseria, G. E.; Robb, M. A.; Cheeseman, J. R.; Zakrzewski, V. G.; Montgomery, J. A., Jr.; Stratmann, R. E.; Burant, J. C.; Dapprich, S.; Millam, J. M.; Daniels, A. D.; Kudin, K. N.; Strain, M. C.; Farkas, O.; Tomasi, J.; Barone, V.; Cossi, M.; Cammi, R.; Mennucci, B.; Pomelli, C.; Adamo, C.; Clifford, S.; Ochterski, J.; Petersson, G. A.; Ayala, P. Y.; Cui, Q.; Morokuma, K.; Malick, D. K.; Rabuck, A. D.; Raghavachari, K.; Foresman, J. B.; Cioslowski, J.; Ortiz, J. V.; Stefanov, B. B.; Liu, G.; Liashenko, A.; Piskorz, P.; Komaromi, I.; Gomperts, R.; Martin, R. L.; Fox, D. J.; Keith, T.; Al-Laham, M. A.; Peng, C. Y.; Nanayakkara, A.; Gonzalez, C.; Challacombe, M.; Gill, P. M. W.; Johnson, B. G.; Chen, W.; Wong, M. W.; Andres, J. L.; Head-Gordon, M.; Replogle, E. S.; Pople, J. A. *Gaussian 98*, revision A.9; Gaussian, Inc.: Pittsburgh, PA, 1998.

(23) Zhang, Y.; Mao, J.; Godbout, N.; Oldfield, E. *J. Am. Chem. Soc.* **2002**, *124*, 13921−13930.

(24) Godbout, N.; Havlin, R.; Salzmann, R.; Debrunner, P. G.; Oldfield, E. *J. Phys. Chem. A* **1998**, *102*, 2342−2350.

(25) Havlin, R. H.; Godbout, N.; Salzmann, R.; Wojdelski, M.; Arnold, W.; Schulz, C. E.; Oldfield, E. *J. Am. Chem. Soc.* **1998**, *120*, 3144−3151.

(26) ADF 2002.01, http://www.scm.com, Theoretical Chemistry, Vrije Universiteit, Amsterdam, The Netherlands.

(27) Dufek, P.; Blaha, P.; Schwarz, K. *Phys. Rev. Lett.* **1995**, *75*, 3545−3548.

(28) AIM2000, version 1.0, written by F. Biegler-König, University of Applied Science, Bielefeld, Germany. Bader, R. F. W. *Atoms in Molecules: A Quantum Theory*; Oxford University Press: Oxford, 1990.

(29) Mao, J.; Zhang, Y.; Oldfield, E. *J. Am. Chem. Soc.* **2002**, *124*, 13911−13920.

(30) Wachters, A. J. H. *J. Chem. Phys.* **1970**, *52*, 1033−1036. Wachters, A. J. H. IBM Technological Report RJ584; 1969. Basis sets were obtained from the Extensible Computational Chemistry Environment Basis Set Database, version 1.0, as developed and distributed by the Molecular Science Computing Facility, Environmental and Molecular Science Laboratory, which is part of the Pacific Northwest Laboratory, P.O. Box 999, Richland, WA 99352, and is funded by the U.S. Department of Energy. The Pacific Northwest Laboratory is a multiprogram laboratory operated by Battelle Memorial Institute for the U.S. Department of Energy under Contract DE-AC06-76RLO 1830. Contact David Feller, Karen Schuchardt, or Don Jones for further information.

(31) Becke, A. D. *Phys. Rev. A* **1988**, *38*, 3098−3100.

(32) Perdew, J. P.; Burke, K.; Wang, Y. *Phys. Rev. B* **1996**, *54*, 16533−16539.

(33) Becke, A. D. *J. Chem. Phys.* **1993**, *98*, 5648−52.

(34) Lee, C.; Yang, W.; Parr, R. G. *Phys. Rev. B* **1988**, *37*, 785−789.

(35) Te Velde, G.; Bickelhaupt, F. M.; Baerends, E. J.; Fonseca Guerra, C.; Van Gisbergen, S. J. A.; Snijders, J. G.; Ziegler, T. *J. Comput. Chem.* **2001**, *22*, 931−967.

(36) Ellison, J. J.; Ruhlandt-Senge, K.; Power, P. P. *Angew. Chem., Int. Ed. Engl.* **1994**, *33*, 1178−1180.

(37) Cerius[2] Modelling Environment, version 4.5, Molecular Simulation Inc., San Diego, CA, 2000.

(38) Holland, P. L.; Cundari, T. R.; Perez, L. L.; Eckert, N. A.; Lachicotte, R. J. *J. Am. Chem. Soc.* **2002**, *124*, 14416−14424.

(39) Schwerdtfeger, P.; Söhnel, T.; Pernpointner, M.; Laerdahl, J. K.; Wagner, F. E. *J. Chem. Phys.* **2001**, *115*, 5913−5924.

(40) Reschke, R.; Trautwein, A.; Desclaux, J. P. *J. Phys. Chem. Solids* **1977**, *38*, 837−841.

(41) Yamada, Y.; Tominaga, T. *J. Radioanal. Nucl. Chem. Lett.* **1994**, *188*, 83. Yamada, Y.; Tominaga, T. *J. Radioanal. Nucl. Chem. Lett.* **1995**, *199*, 95. Yamada, Y.; Tominaga, T. *Radiochim. Acta* **1998**, *80*, 163−170. Yamada, Y. *J. Nucl. Radiochem. Sci.* **2000**, *1*, 75−76. Yamada, Y.; Katsumata, K. *Chem. Lett.* **2000**, 746−747.